Spectral sidebands and multipulse formation in passively mode-locked lasers

Rafi Weill, Alexander Bekker, Vladimir Smulakovsky, and Baruch Fischer
Department of Electrical Engineering, Technion-IIT, Haifa IL-32000, Israel

Omri Gat
Racah Institute of Physics, Hebrew University, Jerusalem IL-91904, Israel
(Received 24 January 2011; published 25 April 2011)

Pulses in passively mode-locked lasers are often accompanied by dispersive waves that form spectral sidebands due to spatial inhomogeneities in the laser cavity. Here we present an explicit calculation of the amplitude, frequency, and precise shape of the sidebands accompanying a solitonlike pulse. We then extend the study to the *global* steady state of mode-locked lasers with a variable number of pulses, and present experimental results in a mode-locked fiber laser that confirm the theory. The strong correlation between the temporal width of the sidebands and the measured spacing between the pulses in a multipulse operation suggests that the sidebands have an important role in the interpulse interaction.

DOI: 10.1103/PhysRevA.83.043831 PACS number(s): 42.55.Wd, 42.60.Fc, 42.55.Ah, 42.65.Sf

I. INTRODUCTION

Short pulses that scatter from periodic spatial inhomogeneities in a dispersive medium emit radiation that interferes constructively at resonant frequencies, forming spectral sidebands, sometimes called Kelly sidebands [1]. Several papers [1–3] studied the formation of dispersive waves by solitons and their propagation in optical fibers with periodically spaced amplifiers. The same mechanism leads to the formation of sidebands in mode-locked lasers, where inhomogeneities in the cavity act periodically on the pulse. Sidebands can also be generated by periodic perturbations of cw [4,5]. The latter type of sidebands arise because of a four-wave-mixing-induced modulational instability, in contrast with the linear resonance responsible for the Kelly sidebands. Recently, sidebands induced by modulational instabilities were also discovered in mode-locked lasers that, unlike Kelly sidebands, occur only beyond a threshold pumping intensity [6].

When the peak power of a single pulse exceeds that of maximal transmissivity, the steady state of a passively mode-locked laser tends to bifurcate into configurations where two or more pulses run in the laser cavity simultaneously [7]. Since the early experiments that demonstrated multipulse mode locking [8–10], it has been observed that the pulses display a very rich dynamics, often forming bunches, as a consequence of complex interpulse interactions. The interest in the dispersive waves in mode-locked lasers, beyond their prominent effect on the pulse shape, arises because they have often been suggested as a means of interpulse interaction in multipulse mode-locked lasers [11–14]. Here, we focus on the steady-state structure of the dispersive waves and the corresponding Kelly sidebands formed by the radiation emitted from the pulses in multipulse mode-locked lasers.

The peak clamping leading to multipulse steady states is often modeled by adding a quintic term to the equations of motion. In former papers [15,16], we applied the statistical light-mode dynamics (SLD) theory to this system, and showed that multipulse mode locking is, in effect, a series of first-order phase transitions. SLD uses the methods of statistical physics to analyze the dynamics of the interacting many-body light-mode system at an effective finite temperature generated by cavity noise [17–19]. Here, we apply the SLD gain balance method [20] to derive the multipulse steady states with dispersive waves of mode-locked lasers with cavity inhomogeneities.

Our theoretical analysis is based on the master equation of mode-locked soliton lasers [21,22], with an additive noise term [23], where the inhomogeneities in the cyclic light propagation in the cavity are modeled by a periodic modulation of the gain and the saturable absorption. We first study the sidebands in a single-pulse steady state and show that, unlike free fiber sidebands, the mode-locked-laser sidebands reach a steady state with a well-defined bandwidth and a Lorentzian shape; in real time, the dispersive waves form a wide pedestal with exponentially decaying tails. In particular, we demonstrate how the overall phase of each sideband depends on the relative phase of the gain and loss modulations. The theory is firmly supported by experimental observations in mode-locked fiber lasers.

Next, we derive a nonlinear equation for the global steady state of the laser, which includes a number of pulses and their accompanying pedestals, by applying the gain balance principle to the pulses, sidebands, and cw components of the waveform. We find that the sideband intensity and the pedestal width increase by a large factor when the pumping is increased with a constant number of pulses, and then decrease abruptly when another pulse is formed, so the properties of single-pulse sidebands display an oscillatory, approximately periodic, dependence on the pump power. These theoretical results are again favorably compared with experiments in a mode-locked fiber laser. We conclude by considering the implication of our results on the nature of sideband-mediated interactions.

II. THEORETICAL MODEL

The mode-locking master-equation model for soliton lasers [21,22,24], where the dominant dynamical processes are

chromatic dispersion and Kerr nonlinearity, takes the form

$$i\partial_z\psi = -\partial_t^2\psi - 2|\psi|^2\psi + ip_g(z)g[\psi]\left(\psi + \gamma\partial_t^2\psi\right) + ip_s(z)(s(|\psi|^2) - l)\psi + \Gamma(z,t). \quad (1)$$

The first two terms on the right-hand side are the aforementioned dispersion and Kerr nonlinearity, the coefficients of which are nondimensionalized by an appropriate choice of units of time and power. The next term models the saturable gain of the laser amplifier. $g[\psi]$ is the overall gain coefficient, and the square brackets signify that g depends on the entire waveform $\psi(t)$ rather than the instantaneous value of ψ only, and γ is the coefficient of parabolic spectral filtering. We will assume that the the gain saturation is slow compared to the cavity round-trip time t_R, so g is determined by the overall power $P = \int_{-t_R/2}^{t_R/2}|\psi|^2 dt$ in the usual manner:

$$g[\psi] = \frac{g_0}{1 + P/P_s}, \quad (2)$$

where g_0 and P_s are the small signal gain and the saturation power, respectively.

The next term on the right-hand side of the master equation models the fast saturable absorber with transmissivity $s(|\psi|) - l$, where l is the small signal loss and $s(0) = 0$ by definition. We do not assume a particular form for the transmissivity function other than that it increases linearly at zero, $s'(0) > 0$. We assume, for simplicity, that the saturable absorber accounts for all the losses in the cavity. The final term is a Gaussian white noise source with covariance

$$\langle\Gamma^*(z,t)\Gamma(z',t')\rangle = 2T\delta(z - z')\delta(t - t'), \quad (3)$$

where the constant T is the rate of internal and injected noise power. As mentioned above, the noise is a significant factor in the determination of the steady state; we conjecture that it is also an essential ingredient in the interpulse interaction. The sidebands are formed by the spatial inhomogeneity of the gain and loss processes in the laser, described by $p_g(z)$ and $p_s(z)$, respectively, which are periodic functions of the cavity round-trip length L, normalized to $\frac{1}{L}\int_0^L dz p_{g,s} dz = 1$.

The dominance of the dispersive effects means that the gain and loss terms in Eq. (1) are proportional to a small parameter, and that the noise term is proportional to an independent small parameter. In spite of their smallness, the gain, loss, and noise are the crucial terms for the mode-locking phenomena discussed here. At the same time, they also perturb the pulse properties that are dominated by the dispersive terms; these small perturbations will be neglected.

III. SINGLE-PULSE SIDEBANDS

We begin our analysis assuming conditions under which there is a single pulse in the cavity with fixed parameters in the steady state. Since the dominant terms in the master equation are the dispersion and Kerr effect, the pulse waveform is approximately that of a nonlinear Schrödinger (NLS) soliton. Solitons are defined by four parameters: amplitude a, frequency, timing, and phase. The gain and loss terms in the master equation fix the frequency to zero, and we can set the timing and phase to zero by an appropriate choice of origin, so the soliton waveform is

$$\psi_p(t,z) = a\ \mathrm{sech}(at)e^{ia^2z}. \quad (4)$$

The soliton waveform ψ_p is not an exact solution of the master equation because of the gain, loss, and noise terms. We therefore look for a solution of the form

$$\psi(t,z) = \psi_p(t,z) + \psi_b(t,z) + \psi_c(t,z), \quad (5)$$

which, in addition to the pulse waveform, consists of the sideband waveform ψ_b generated as a result of scattering of the pulses off the cavity inhomogeneities, and the continuum ψ_c generated by the cavity noise. The three waveform components have different characteristic time scales: the sidebands are narrow resonances, the temporal width of which is, as shown below, inversely proportional to the gain-loss small parameter. This width is large compared with the pulse width, but small compared with the cavity round-trip time, i.e., the scale of the continuum.

Both ψ_b and ψ_c have low peak power and can therefore be analyzed by the linearized master equation, although their total power $\int dt|\psi_b|^2$, $\int dt|\psi_c|^2$ can be of the order P. The effect of noise is negligible on ψ_b, which therefore satisfies the equation

$$\partial_z\psi_b = i\left(\partial_t^2\psi_b + 4|\psi_p|^2\psi_b + 2\psi_p^2\psi_b^*\right) + p_g(z)g[\psi]\left(1 + \gamma\partial_t^2\right)(\psi_p + \psi_b) + p_p(z)(s(|\psi_p|^2) - l)(\psi_p + \psi_b). \quad (6)$$

The right-hand side of Eq. (6) retains terms that are of higher order of smallness than ψ_b; these terms are, in effect, not negligible for $|t| \gg a$ where ψ_p is itself small, and play a crucial role in the shaping of the sidebands, as shown below.

The discrete modes of the real linear Eq. (6) express small variations of the pulse parameters [23,25], while ψ_b, which consists of radiation emitted by the pulse, is a linear combination

$$\psi_b(t,z) = e^{ia^2z}\int\frac{d\omega}{2\pi}[\alpha_\omega(z)u_\omega(t) + \alpha_\omega(z)^* v_\omega(t)^*] \quad (7)$$

of the first component of the scattering states of the linear operator L,

$$L\begin{pmatrix}u_\omega\\ v_\omega\end{pmatrix} = [-(i + g\gamma)\omega^2 - ia^2]\begin{pmatrix}u_\omega\\ v_\omega\end{pmatrix}, \quad (8)$$

$$L\begin{pmatrix}v_\omega^*\\ u_\omega^*\end{pmatrix} = [(i - g\gamma)\omega^2 + ia^2]\begin{pmatrix}v_\omega^*\\ u_\omega^*\end{pmatrix}, \quad (9)$$

which acts on two-component wave functions as

$$L = \begin{pmatrix}A & B\\ B^* & A^*\end{pmatrix} \quad (10)$$

with

$$A = (i + g\gamma)\partial_t^2 - ia^2 + 4ia^2\mathrm{sech}^2(at) + s[a^2\mathrm{sech}^2(at)]$$

and $B = 2ia\mathrm{sech}^2(at)$. It will be argued below that we can approximate the space-dependent linear operator acting on ψ_b

in Eq. (6) by its space average L. Within this approximation, the coefficients defined in Eq. (7) evolve according to

$$\partial_z \alpha_\omega = [-(i+g\gamma)\omega^2 - ia^2]\alpha_\omega + (g\alpha_\omega + \beta_{g\omega})p_g(z) + (-l\alpha_\omega + \beta_{s\omega})p_s(z), \tag{11}$$

where β_g and β_s are the expansion coefficients of the forcing terms $g(1+\gamma\partial_t^2)[a\,\mathrm{sech}(at)]$ and $\{s[a^2\mathrm{sech}^2(at)] - l\}$ $a\mathrm{sech}(at)$, respectively. As usual, the expansion coefficients are extracted by the inner product with the adjoint eigenfunctions defined by

$$L^\dagger \begin{pmatrix} \bar{u}_\omega \\ \bar{v}_\omega \end{pmatrix} = [(i-g\gamma)\omega^2 + ia^2](\omega^2 + a^2)\begin{pmatrix} \bar{u}_\omega \\ \bar{v}_\omega \end{pmatrix}, \tag{12}$$

$$L^\dagger \begin{pmatrix} \bar{v}^*_\omega \\ \bar{u}^*_\omega \end{pmatrix} = [-(i+g\gamma)\omega^2 - ia^2]\begin{pmatrix} \bar{v}^*_\omega \\ \bar{u}^*_\omega \end{pmatrix} \tag{13}$$

normalized so that

$$\int dt[\bar{u}_\omega(t)^* u_{\omega'}(t) + \bar{v}_\omega(t)^* v_{\omega'}(t)] = 2\pi\delta(\omega - \omega'), \tag{14}$$

$$\int dt[\bar{v}_\omega(t) u_{\omega'}(t) + \bar{u}_\omega(t) v_{\omega'}(t)] = 0. \tag{15}$$

Since, by assumption, the dispersive terms are dynamically dominant, the eigenfunctions of L are close to the eigenfunctions of the linearized NLS equation [26]

$$u_\omega(t) = e^{i\omega t}\left(1 - \frac{2i\omega e^{-at}}{(\omega+ia)^2}a\mathrm{sech}(at) + \frac{a^2\mathrm{sech}^2(at)}{(\omega+ia)^2}\right), \tag{16}$$

$$v_\omega(t) = e^{i\omega t}\frac{a^2\mathrm{sech}^2(at)}{(\omega+ia)^2}, \tag{17}$$

$$\bar{u}_\omega(t) = a\frac{(\omega+ia)^2}{(\omega-ia)^2}u_{-\omega}(-t), \tag{18}$$

$$\bar{v}_\omega(t) = -a\frac{(\omega+ia)^2}{(\omega-ia)^2}v_{-\omega}(-t), \tag{19}$$

so that

$$\beta_{g\omega} = \frac{a}{2\pi}\frac{(\omega+ia)^2}{(\omega-ia)^2}\int dt\left(1+\gamma a^2\partial_\theta^2\right)a\,\mathrm{sech}\theta \times e^{-i\omega t}\left(1 - \frac{2i\omega e^{-at}a\mathrm{sech}(at) + a^2\mathrm{sech}^2(at)}{(\omega+ia)^2}\right), \tag{20}$$

$$\beta_{s\omega} = \frac{a}{2\pi}\frac{(\omega+ia)^2}{(\omega-ia)^2}\int dt\{s[a^2\mathrm{sech}^2(at)] - l\}a\mathrm{sech}(at) \times e^{-i\omega t}\left(1 - \frac{2i\omega e^{-at}a\mathrm{sech}(at) + a^2\mathrm{sech}^2(at)}{(\omega+ia)^2}\right). \tag{21}$$

The solution of Eq. (11) is

$$\alpha_\omega(z) = \int^z dz' e^{[-\omega^2(i+g\gamma) - ia^2](z-z')} \times e^{\int_{z'}^z dz''[gp_g(z'') - lp_s(z'')]}[\beta_{g\omega}p_g(z') + \beta_{s\omega}p_s(z')]. \tag{22}$$

As observed by Gordon and Kelly [1–3], the amplitudes α_ω are driven resonantly if the nonlinear frequency shift $a^2 + \omega^2$ is an integer multiple of the cavity-based wavelength $\frac{2\pi}{L}$; spectrally, therefore, the dispersive waves contain a discrete set of sidebands at frequencies $\pm\omega_n$:

$$\omega_n = \sqrt{\frac{2\pi}{L}n - a^2}, \quad n = 1,2,\ldots. \tag{23}$$

The nth sideband is forced mainly by the nth harmonic of the gain and loss modulation functions $p_{g,l}$, but also by the z dependence of the gain and loss terms in the exponent in Eq. (22). The latter modulation is small, however, if we make the simplifying assumption that the total net loss per round trip is small, so the z' integration in Eq. (22) is effective over many round trips. This is the usual assumption underlying the Haus master equation [21] and is also consistent with the relative weakness of the gain and loss processes in the dynamics dominated by the chromatic dispersion and Kerr nonlinearity that is studied here.

In this case, the mean net loss in the z'' integration in Eq. (22) dominates over the variable parts of the gain and loss, and the latter may be neglected. The same assumption justifies the approximation of the time-dependent linear operator in Eq. (6), the equation of motion for ψ_b, by the fixed operator L that was used to derive Eq. (11).

It now follows that the dispersive wave amplitudes are

$$\alpha_\omega(z) = \int^z dz' e^{[-i(a^2+\omega^2)+g(1-\gamma\omega^2)-l](z-z')} \times [\beta_{g\omega}p_g(z') + \beta_{s\omega}p_s(z')] \tag{24}$$

and defining the nth Fourier components $\tilde{p}_{g,n}$ and $\tilde{p}_{s,n}$ of p_g and p_s, respectively, the coefficients of the nth sideband in the steady state are

$$\alpha_{\omega,n}(z) = \frac{(\tilde{p}_{g,n}\beta_{g\omega} + \tilde{p}_{s,n}\beta_{s\omega})\,e^{-\frac{2\pi}{L}inz}}{l + g(\gamma\omega^2 - 1) + i\left(\omega^2 - \omega_n^2\right)}. \tag{25}$$

We wish to characterize the sidebands by their ordinary Fourier spectrum, obtainable from Eq. (7),

$$\tilde{\psi}_{bn}(\omega,z) = e^{ia^2z}\int\frac{d\omega'}{2\pi}[\alpha_{n\omega'}(z)\tilde{u}_{\omega'\omega} + \alpha_{n,\omega'}(z)^*\tilde{v}^*_{\omega'\omega}], \tag{26}$$

where $\tilde{u}_{\omega'\omega} = \int dt\, e^{-i\omega t}u_{\omega'}(t)$, and $\tilde{v}_{\omega'\omega}$ is defined similarly. As a transform of a rapidly varying function, $\tilde{u}$ is wideband (its ω bandwidth for fixed ω' is comparable with the soliton bandwidth), but it is also singular for $\omega = \omega'$. The smooth part of $\tilde{u}$ generates a small deformation of the soliton waveform in Eq. (26), which is unimportant for the present purpose of characterizing the sideband spectrum. We therefore focus on the singular part $\check{u}_{\omega'\omega}$ of $\tilde{u}_{\omega'\omega}$, which is determined by the $\pm\infty$ asymptotes of $u_{\omega'}$ [see Eq. (16)] to

$$\check{u}_{\omega'\omega} = 2\pi\frac{\omega^2-1}{(\omega+ia)^2}\delta(\omega-\omega') + \frac{4\omega a}{(\omega+ia)^2}\mathrm{P}\frac{1}{\omega-\omega'}, \tag{27}$$

where P denotes principal part. $\check{v}_{\omega'\omega} = 0$ since $v_\omega(t)$ tends to zero exponentially for $t \to \pm\infty$.

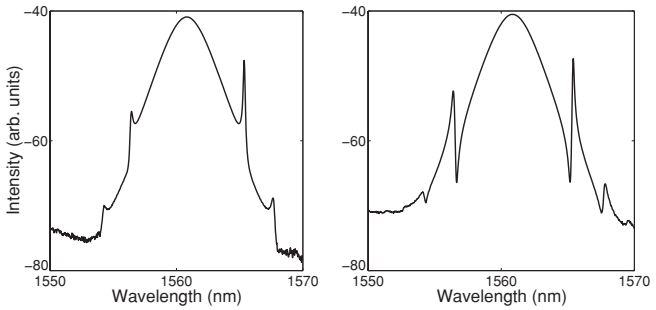

FIG. 1. Measured spectra of the soliton and its sidebands, showing the notch formation. The two figures correspond to two measurement locations in the same cavity that are separated by one quarter of cavity length. These measurements agree well with the theory.

Now we can carry out the ω' integration in Eq. (26) and obtain the spectrum of the nth sideband

$$\tilde{\psi}_{b,n}(\omega) = \frac{(\tilde{p}_{g,n}\beta_{g\omega} + \tilde{p}_{s,n}\beta_{s\omega})\, e^{i(a^2 - \frac{2\pi}{L}n)z}}{l + g(\gamma\omega^2 - 1) + i\left(\omega^2 - \omega_n^2\right)}. \tag{28}$$

The spectral width (half width at half maximum) of the sideband is given by $\delta\omega = [l + g(\gamma\omega_n^2 - 1)]/2\omega_n \ll 1$; temporally, therefore, the dispersive wave is a pedestal of frequency ω_n with an exponentially decaying envelope centered at the pulse, the decay time scale of which is much wider than the soliton width.

Experimentally, the sidebands appear as a series of sharp peaks in the pulse spectrum on the background of the wide soliton spectrum (see Fig. 1). A distinctive feature of the sideband spectrum (28) is the dependence of the overall phase of the sideband on the measurement position in the cavity; as a consequence, the sideband spectrum interferes constructively or destructively with the soliton spectrum, depending on the placement of the output coupler, exhibiting a sharp notch feature for some placements as the result of destructive interference. Figures 1 and 2 show the comparison between the measurement and calculation of the soliton and the first two sidebands' spectrum for two cavity positions. The good agreement between theory and experiment, and the fact that the sidebands are observed for all pumping strengths that allow mode locking, demonstrate that these are indeed Kelly sidebands The main qualitative discrepancy between theory and experiment is the asymmetry between the left and right sidebands, which is lacking in the theory. The most likely source of this asymmetry is the asymmetry of the spectral net gain curve with respect to the band center [27] and the resultant frequency pulling [28], which are not included in our model for simplicity.

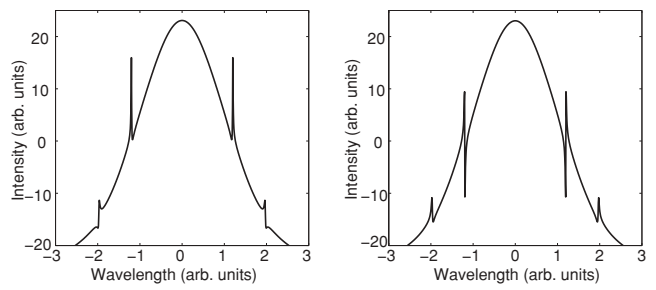

FIG. 2. Theoretical calculation of the pulse and sideband spectrum with $a = 1, g = 0.1, \gamma = 0.01, l = 0.11, s = 0.1(|\psi|^2 - |\psi^4|), t_R T = 10^{-3}, L = 2.56, \tilde{p}_g = e^{i\pi/2}$, and $\tilde{p}_s = e^{i\pi}$. The cavity position in the left figure is $z = L/5$, and in the right is $z = 0$.

IV. THE CONTINUUM COMPONENT

The continuum ψ_c is the dominant component of the waveform for most of its temporal extent, where both $\psi_p(t)$ and $\psi_b(t)$ are negligible. Therefore, the nonlinearity and interaction with the pulses are unimportant for its dynamics, and it is natural to express it in terms of the ordinary Fourier modes $\tilde{\psi}_c(\omega)$ that satisfy

$$\partial_z \tilde{\psi}_c = -i\omega^2 \tilde{\psi}_c + p_g(z) g(1 - \gamma\omega^2)\tilde{\psi}_c - p_s(z) l \tilde{\psi}_c + \tilde{\Gamma}(\omega, z). \tag{29}$$

Because the noise and continuum extend throughout the entire round-trip time, we must use discrete frequencies to label their Fourier transform. It then follows from Eq. (3) that $\tilde{\Gamma}(\omega,z) = \int dt e^{-i\omega t}\Gamma(t,z)$ has zero mean and correlation function $\langle \tilde{\Gamma}(\omega,z)\tilde{\Gamma}^*(\omega',z')\rangle = 2T t_R \delta(z - z')\delta_{\omega,\omega'}$. The solution of Eq. (29) is similar to that of (22), and, by the same arguments that lead to Eq. (24), we again approximate the integrand in the exponent by its mean value. The resulting expression implies that $\langle \tilde{\psi}_c(\omega)\rangle = 0$ and

$$\langle \tilde{\psi}_c(\omega)\tilde{\psi}_c^*(\omega')\rangle = \frac{t_R T \delta_{\omega,\omega'}}{l + g(\gamma\omega^2 - 1)}. \tag{30}$$

V. GAIN BALANCE AND MULTIPULSE SIDEBANDS

In the analysis presented so far, the pulse parameters and the overall saturated gain g were assumed fixed and given. In the steady state, these are variables determined along with the number of pulses as a solution of the optical equation of motion [Eq. (1)]. Since the equation of motion is random, the result is a *statistical* steady state. In previous works [19,20], statistical light-mode dynamics (SLD) theory was used to study this problem and applied to multipulse mode locking in [15,16]. The global mode-locking analysis determines, in particular, the properties of the sidebands, and in this way allows us to reach our goal of describing the width and power of the sidebands as a function of the laser parameters.

Here we study the statistical steady state by the gain balance method, deriving equations of motion for the power in the three components of the optical waveform, that is, the power P_p in the pulse waveform that comprises zero or more pulses, the sidebands power P_b, and the continuum power P_c. The three waveform components are characterized by well-separated time scales, and the total power can therefore be calculated as a sum of the powers of the individual components. One looks for a steady state where the three components are subject to the same saturated gain, and finally the gain itself is determined self-consistently from Eq. (2).

We will assume that the multipulse waveform is of the simplest kind [15], which is also the most commonly observed experimentally, consisting of k pulses of equal amplitude a. In the equation of motion for the pulse amplitude, we may neglect

the noise term in the master equation, and use the results of soliton perturbation theory [3,29] to write

$$\frac{da}{dz} = \mathrm{Re}\int dt\,\psi_p^*\{gp_g(z)(1+\gamma_g\partial_t^2)\psi_p + p_s(z)[s(|\psi_p|^2)-l]\psi_p\} = 2gp_g(z)a\left(1-\frac{\gamma}{3}a^2\right)+p_s(z)[2s_a(a)-2l]a, \quad (31)$$

where

$$s_a(a) = \frac{1}{2a}\int s[a^2\mathrm{sech}^2(at)]a^2\mathrm{sech}^2(at)\,dt. \quad (32)$$

The pulse amplitude changes periodically during its propagation in the cavity; for our purposes, we need the mean pulse amplitude $\bar{a}(z) = \frac{1}{L}\int a(z+z')dz'$. Under the assumption of weak gain and loss processes, the dynamics of $\bar{a}$ is obtained by the space average of Eq. (31), which gives in the steady state

$$g\left(1-\frac{\gamma}{3}\bar{a}^2\right) - l + s_a(\bar{a}) = 0. \quad (33)$$

This equation, together with $P_p = 2k\bar{a}$, determines the pulse part of the gain balance.

Next, we calculate the power carried by the pedestals of the pulses. Each pulse generates a series of sidebands of the form given by Eq. (28). The sidebands power is dominated by the leading $n = \pm 1$ sidebands; since the different pulses that act as sources for the sidebands are not phase locked, we treat them as incoherent sources, and accordingly calculate the total sidebands power as the sum of the individual sideband powers. The resulting expression is

$$P_b = k\frac{\left|\tilde{p}_{g,1}\beta_{g\omega_1}+\tilde{p}_{s,1}\beta_{s\omega_1}\right|^2}{2\omega_1\left[l+g\left(\gamma\omega_1^2-1\right)\right]}. \quad (34)$$

Finally, the mean power of the the continuum is not changed by the presence of the sidebands, and is therefore given by the expression derived in [30]

$$P_c = \frac{Tt_R}{2\sqrt{g\gamma(l-g)}}. \quad (35)$$

We now substitute $P = P_p + P_b + P_c$ into Eq. (2) and obtain a nonlinear equation for the saturated gain g, which is easy to solve numerically. Once we know the value of g, we obtain the steady-state solution of the entire waveform. The steady-state equation can have several solutions with different numbers of pulses k. In such cases, the laser waveform can exist in several states [15,16] in a similar manner to the existence of metastable phases in thermodynamic systems undergoing first-order phase transitions. The laser then exhibits hysteresis; its actual state depends on the history.

Figures 3 and 4 show the results of the calculation as the small signal gain g_0 is varied. For very low gain, the waveform is pure continuum, and its energy increases with the gain. When g_0 is increased beyond a certain threshold, a pulse forms and along with it also a dispersive wave. Because of gain saturation, the net gain must abruptly decrease, and along with it also the continuum component. Further increase of g_0 will mainly increase the sidebands and the continuum components, and slightly change the pulse amplitude, until the second threshold is met; then, the continuum as well as the sidebands' power abruptly decrease again. This process then continues periodically when further pulse creation thresholds are reached. In addition, as the pumping is increased between pulse creation thresholds, the saturated gain increases, so the net loss decreases and the sidebands become spectrally narrower and, accordingly, temporally wider.

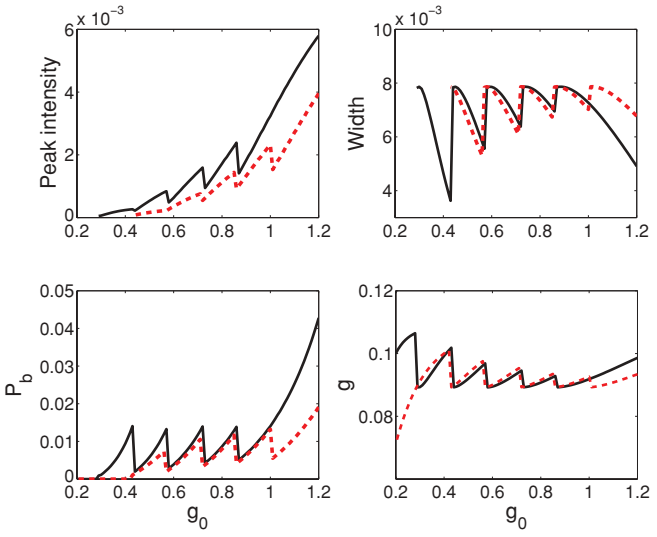

FIG. 3. (Color online) The theoretical calculated values of the sidebands peak intensity, width, and total power P_b along with the saturated gain coefficient g as a function of the small signal gain g_0. The same parameters as in Fig. 2 were used in the calculation, except that $\gamma = 10^{-3}$ and $P_s = 1$. Two noise injection rate values are shown: $T = 10^{-3}$ in the continuous black line and $T = 3\times10^{-3}$ in the dashed red line. The number of pulses is indicated. All values are given in natural soliton units.

The theoretical predictions of the global sideband characteristics agree well with experimental observation summarized in Fig. 5, made on a fiber ring laser mode locked by polarization rotation as described in [16]. In both graphs, the sideband width displays roughly periodic sawtooth behavior and the total sideband energy displays a sawtooth behavior

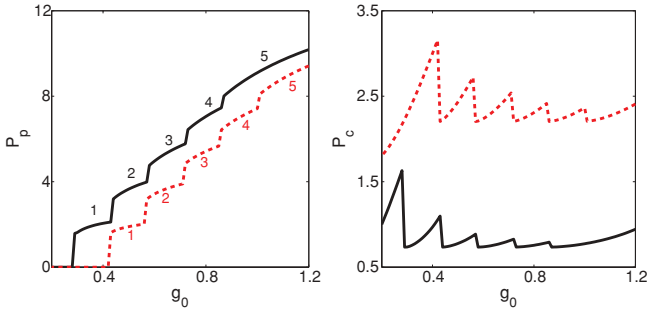

FIG. 4. (Color online) The theoretical calculated values of the total pulse power P_p and continuum power P_c as a function of the small signal gain g_0. The same parameters are used as in Fig. 3. The number of pulses is indicated. All values are given in natural soliton units.

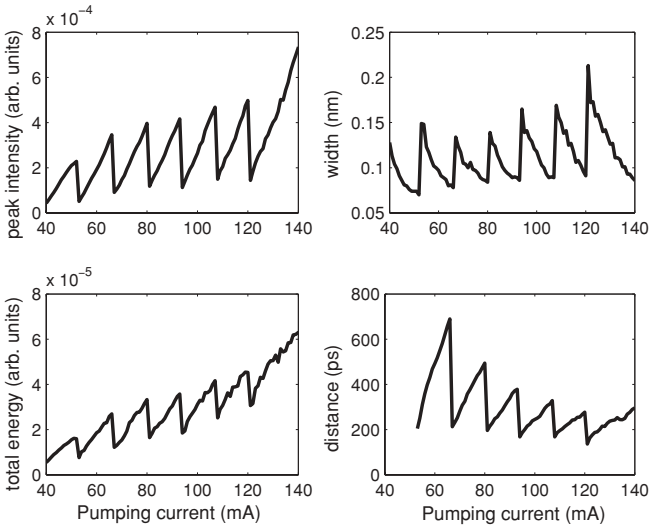

FIG. 5. The measured sideband spectrum characteristics: peak power (in arbitrary units), spectral width, and total energy (in arbitrary units), and the distance between adjacent pulses in states with two or more pulses.

with an increasing linear bias. There is somewhat worse agreement in the peak intensity, but this quantity is sensitive to interferometric enhancement and reduction as explained above.

In both theory and experiments, the spectral width of the sidebands narrows with increasing pumping between pulse creation thresholds, implying a temporal widening of the pedestals. This widening shows a striking correlation with the increase of the interpulse distance, suggesting that the sidebands play a role in the interpulse interactions [12,13].

VI. CONCLUSIONS AND OUTLOOK

We presented a fundamental theory of the formation of sidebands and their effect on the statistical steady state in multipulse mode-locked soliton lasers, which explains the main experimental observations, including the dependence of the sideband spectrum on the measurement position in the cavity, the growth of the sideband energy and temporal width when pumping is increased, and the abrupt attenuation of the sidebands when a new pulse is created in the cavity. We also found strong correlations between the temporal width of the sidebands and the spacing between adjacent pulses in pulse bunches, giving further evidence for the role of the sidebands in interpulse interaction. However, the most natural conclusion from our observation is that the sidebands generate *repulsive* interactions, and that additional attractive interactions are needed to explain the ubiquitous formation of pulse bunches. Moreover, the phase and timing jitter of the pulses leads us to conjecture that the mechanism of interaction is incoherent. We postpone the in-depth study of these questions to a future publication.

ACKNOWLEDGMENT

This research was supported by the Israel Science Foundation.

[1] S. M. J. Kelly, Electron. Lett. **28**, 806 (1992).
[2] J. N. Elgin and S. M. J. Kelly, Opt. Lett. **18**, 787 (1993).
[3] J. P. Gordon, J. Opt. Soc. Am. B **9**, 91 (1992).
[4] F. Matera, A. Mecozzi, M. Romagnoli, and M. Settembre, Opt. Lett. **18**, 1499 (1993).
[5] N. J. Smith and N. J. Doran, Opt. Lett. **21**, 570 (1996).
[6] D. Y. Tang, L. M. Zhao, X. Wu, and H. Zhang, Phys. Rev. A **80**, 023806 (2009).
[7] D. Y. Tang, L. M. Zhao, B. Zhao, and A. Q. Liu, Phys. Rev. A **72**, 043816 (2005).
[8] M. Nakazawa, E. Yoshida, and Y. Kimura, Appl. Phys. Lett. **59**, 2073 (1991).
[9] D. J. Richardson, R. I. Laming, D. N. Payne, M. W. Phillips, and V. J. Matsas, Electron. Lett. **27**, 730 (1991).
[10] A. B. Grudinin, D. J. Richardson, and D. N. Payne, Electron. Lett. **28**, 67 (1992).
[11] D. Y. Tang *et al.*, Phys. Rev. E **72**, 016616 (2005).
[12] J.-M. Soto-Crespo, N. Akhmediev, Ph. Grelu, and B. Belhache, Opt. Lett. **28**, 1757 (2003).
[13] A. B. Grudinin and S. Gray, J. Opt. Soc. Am. B **14**, 144 (1997).
[14] A. Komarov, K. Komarov, and F. Sanchez, Phys. Rev. A **79**, 033807 (2009).
[15] B. Vodonos, R. Weill, A. Gordon, A. Bekker, V. Smulakovsky, O. Gat, and B. Fischer, Phys. Rev. Lett. **93**, 153901 (2004).
[16] R. Weill, B. Vodonos, A. Gordon, O. Gat, and B. Fischer, Phys. Rev. E **76**, 031112 (2007).
[17] A. Gordon and B. Fischer, Phys. Rev. Lett. **89**, 103901 (2002).
[18] A. Gordon and B. Fischer, Opt. Commun. **223**, 151 (2003).
[19] O. Gat, A. Gordon, and B. Fischer, Phys. Rev. E **70**, 046108 (2004).
[20] M. Katz, A. Gordon, O. Gat, and B. Fischer, Phys. Rev. Lett. **97**, 113902 (2006).
[21] H. A. Haus, IEEE J. Sel. Top. Quantum Electron. **6**, 1173 (2000).
[22] J. N. Kutz, SIAM Rev. **49**, 629 (2006).
[23] H. A. Haus and A. Mecozzi, IEEE J. Quantum Electron. **29**, 983 (1993).
[24] H. A. Haus, J. Appl. Phys. **46**, 3049 (1975).
[25] M. Katz, O. Gat, and B. Fischer, Opt. Lett. **35**, 297 (2010).
[26] D. J. Kaup, Phys. Rev. A **42**, 5689 (1990).
[27] W. S. Man, H. Y. Tam, M. S. Demokan, P. K. A. Wai, and D. Y. Tang, J. Opt. Soc. Am. B **17**, 28 (2000).
[28] C. R. Menyuk, J. K. Wahlstrand, J. Willits, R. P. Smith, T. R. Schibli, and S. T. Cundiff, Opt. Express **15**, 6677 (2007).
[29] V. I. Karpman, Phys. Scr. **20**, 462 (1979).
[30] O. Gat, A. Gordon, and B. Fischer, New J. Phys. **7**, 151 (2005).